

# Neutrino Oscillation Search at MiniBooNE

Z. Djurcic\* for the MiniBooNE Collaboration <sup>a†</sup>

<sup>a</sup>Columbia University, New York, NY 10027, USA

This article reports the status of a  $\nu_\mu \rightarrow \nu_e$  oscillation search in MiniBooNE (Booster Neutrino Experiment) experiment. If an appearance signal is observed, it will imply Physics Beyond the Standard Model such as the existence of light sterile neutrino.

## 1. INTRODUCTION

In recent years, the solar-neutrino [1], reactor-neutrino [2], atmospheric-neutrino [3], and accelerator-neutrino [4] experiments have confirmed the existence of neutrino oscillations. These results implied the existence of two independent  $\Delta m^2$  regions, with  $\Delta m^2 \sim 8 \times 10^{-5} eV^2$  in the solar, and with  $\Delta m^2 \sim 3 \times 10^{-3} eV^2$  in the atmospheric sector. The Standard Model incorporates two separate oscillation regions with three known neutrino flavors:  $\nu_e$ ,  $\nu_\mu$ , and  $\nu_\tau$ . However, an unconfirmed evidence for neutrino oscillations came from the LSND [5] experiment with  $\Delta m^2$  at  $\sim 1 eV^2$  value. The discovery of nonzero neutrino masses through the neutrino oscillations has raised a number of very interesting questions about the neutrinos and their connections to other areas of physics and astrophysics. One question is whether there are sterile neutrinos that do not participate in the standard weak interactions. This question is primarily being addressed by the MiniBooNE experiment. The MiniBooNE experiment will confirm or refute the LSND result with higher statistics and different sources of systematic error. If the LSND neutrino oscillation evidence is confirmed, it will, together with solar, reactor, atmospheric and accelerator oscillation data, imply Physics Beyond the Standard Model such as the existence of light sterile neutrino [6]. While LSND observed an excess of  $\bar{\nu}_e$  events in a  $\bar{\nu}_\mu$  beam, MiniBooNE is a  $\nu_\mu \rightarrow \nu_e$  search.

## 2. THE EXPERIMENT

MiniBooNE is a fixed target experiment currently taking data at Fermi National Accelerator Laboratory. The neutrino beam is produced from 8.89 GeV/c protons impinging on a 71 cm long and 1 cm diameter beryllium target. The target is located inside a magnetic focusing horn that increases the neutrino flux at the detector by a factor of  $\sim 5$ , and can operate in both negative and positive polarities for  $\nu$  and  $\bar{\nu}$  running. MiniBooNE collected approximately  $6 \times 10^{20}$  protons on target (POT) in neutrino mode. This data sample is currently used in the neutrino oscillation analysis. Mesons produced in the target decay-in-flight in a 50 m long decay pipe. The neutrino beam is composed of  $\nu_\mu$  from  $K^+/\pi^+ \rightarrow \mu^+ + \nu_\mu$  decays. The neutrino beam propagates through a 450 m of a dirt absorber before entering the detector. There is a small contamination from  $\nu_e$ . The processes that contribute to the intrinsic  $\nu_e$  in the beam are  $\mu^+ \rightarrow e^+ \nu_e \bar{\nu}_\mu$ ,  $K^+ \rightarrow \pi^0 e^+ \nu_e$ , and  $K_L^0 \rightarrow \pi^\pm e^\pm \nu_e$ . Early in 2006, MiniBooNE switched the polarity of the horn to select negative sign mesons.

The MiniBooNE detector is a 12.2 m diameter sphere filled with 800 tons of pure mineral oil. The center of the MiniBooNE neutrino detector is positioned  $L = 541 m$  from the front of the beryllium target. The vessel consists of two optically isolated regions divided by a support structure located at 5.5 m radius. The inner volume is the neutrino target region, while the outer volume forms the veto region. There are 1280 8-inch photo-tubes (PMTs) pointed inward provid-

\*Email address: zdjurcic@nevis.columbia.edu

<sup>†</sup>MiniBooNE Experiment is supported by NSF and DOE.

ing 10% coverage, and 292 outward-faced PMTs in the veto region. Data analysis require a fiducial volume cut at 500 cm from the center of the tank to ensure good event reconstruction, resulting in a 445 ton target region. The outer volume serves as a veto shield for identifying particles both entering and leaving the detector. The rate of neutrino candidates per proton delivered to the target was constant ( $1.089 \times 10^{-15} \nu/\text{POT}$ ) over the period of data acquisition, as demonstrated in Figure 1. Protons delivered to the MiniBooNE

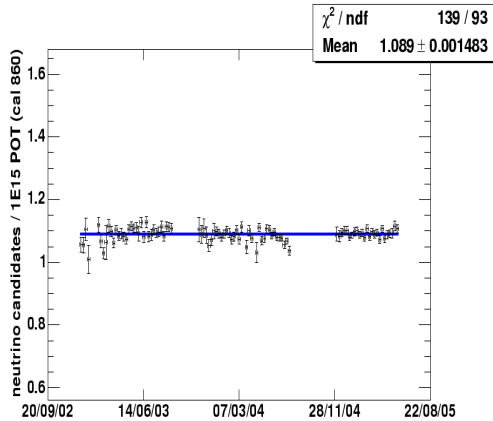


Figure 1. Calibrated neutrino rate per proton on target.

target are monitored by two toroids located in the beam line. The main MiniBooNE trigger is an accelerator signal indicating a beam spill. Every beam trigger opens a  $19.2 \mu\text{s}$  window in which all events are recorded. Other triggers include a supernova trigger, a random strobe trigger for beam-off measurements, a laser calibration trigger, cosmic muon triggers, and a trigger to record neutrino events from the NuMI beam line.

The interaction point, event time, energies, and the particle tracks are recorded from the times and charges of the PMT hits in the detector. Neu-

trino induced events are identified by requiring that the event is observed during the beam spill, have fewer than 6 veto PMT hits, and greater than 200 tank PMT hits. These simple cuts yield a cosmic ray rejection that is better than 1000:1.

The MiniBooNE detector is calibrated using a laser system, cosmic rays and neutrino interactions. The calibration procedures cover the full energy range from 50 to 1000 MeV using different event types. Stopping cosmic ray muons are used to calibrate the energy scale for muon-type events and measure the position and angle reconstruction resolution, when their path length can be identified. This is accomplished with a scintillator hodoscope on the top of the detector, combined with scintillation cubes at various positions within the detector volume. Analysis of the cosmic muons indicates that the energy and angle resolution of muons is 10% and  $6.4^\circ$ , respectively. Observed Michel electrons from muon decay are used to calibrate the energy scale of electron-type events at the 52.8 MeV Michel endpoint, with 12% resolution. Reconstructed  $\pi^0$  events provide another electron-like calibration source. The photons that are emitted in  $\pi^0$  decays span a considerable range to over 1000 MeV. The  $\pi^0$  mass derived from reconstructed energies and directions of two  $\gamma$ -rays has a peak at  $136.3 \pm 0.8 \text{ MeV}$ . The resolution on the reconstructed  $\pi^0$  mass peak is 20 MeV. This is in an excellent agreement with the 135.0 MeV expectation, providing a check on the energy scale and the reconstruction over the full energy range of interest for the  $\nu_e$  appearance analysis.

### 3. NEUTRINO FLUX, CROSS SECTION, AND DETECTOR MODELING

The flux modeling uses a Geant4-based simulation of beam line geometry. Hadron production in the target is based on Sanford-Wang parametrization of  $p - Be$  cross-section, with parameters determined by a global fit to  $p - Be$  particle production data. Simulated neutrino flux has an energy distribution with a peak at  $\sim 0.7 \text{ GeV}$ . Therefore, the average  $L/E_\nu$  ratio is  $\sim 0.8 \text{ km/GeV}$  compared to LSND's  $L/E_\nu \sim 1 \text{ km/GeV}$ .

The NUANCEv3 [7] event-generator simulates

interactions in the detector. The cross section model describes the various neutrino interaction processes on  $CH_2$ , which include the Llewellyn-Smith free nucleon quasi-elastic cross section, the Rein-Seghal resonant and coherent pion production cross section, a Smith-Moniz Fermi gas model, and final state interactions based on  $\pi$ -Carbon scattering data.

The MiniBooNE detector is modeled using an extended GEANT3-based simulation. An extended light propagation model of the detector describes the emission of optical and near-UV photons via Cerenkov radiation and scintillation. Each photon is individually tracked, undergoing scattering, fluorescence, and reflection, until it is absorbed. The response of the electronics to the photoelectrons resulting from photons hitting PMT's is simulated, with the final output being digitized waveforms simulating the charge and time channels of the electronics in a form identical to that used for data.

#### 4. THE BACKGROUNDS IN THE APPEARANCE SIGNAL

The signature of an oscillation event is the  $\nu_e + n \rightarrow e + p$  reaction. The backgrounds in the oscillation analysis are divided in two main categories: intrinsic  $\nu_e$  events in the beam, and  $\nu_\mu$  events that are mis-identified as  $\nu_e$  events.

The beam that arrives at the detector is almost pure  $\nu_\mu$  with a small (0.6%) contamination of  $\nu_e$  coming from muon and kaon decays in the decay pipe. The  $\nu_e$  from  $\mu$ -decay are directly tied to the observed  $\nu_\mu$  interactions. Taking into account a small solid angle subtended by the MiniBooNE detector, the pion energy distribution can be determined from the energy of the observed  $\nu_\mu$  events. The pion energy spectrum is then used to predict the  $\nu_e$  from  $\mu$ -decay. A second source of  $\nu_e$  originates from  $K_{e3}$ -decay. This component is constrained using high energy  $\nu_\mu$  charged current quasi-elastic (CCQE) events, that originate primarily from kaon decays.

Mis-identified  $\nu_\mu$  events are  $\pi^0$ ,  $\Delta$ -decays, and  $\nu_\mu$  CCQE events. Most  $\pi^0$  are identified by the reconstruction of two Cerenkov rings produced by two decay  $\gamma$ -rays, as shown in Figure 2. However,

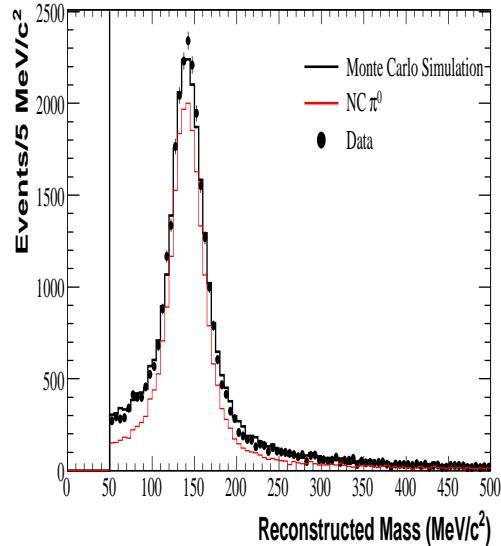


Figure 2. (Preliminary) Mass distribution of  $\pi^0$  candidates obtained using a two ring likelihood fit. The data are the black points, the black line is Monte Carlo simulated neutrino interactions, while the red line is the subset of these events which have at least one  $p\pi^0$  in the final state.

the decay of  $\pi^0$  can appear much like primary electron emerging from a  $\nu_e$  charged current interaction if one of the gammas from the decay overlaps the other, or is too low in energy to be detected. Over 99% of the NC  $\pi^0$  are rejected in the appearance analysis. In addition to its primary decay  $\Delta \rightarrow \pi N$ , the  $\Delta$  resonance has a branching fraction of 0.56% to the  $\gamma N$  final state. The  $\gamma$ -ray may mimic an electron from  $\nu_e$  interaction. The rate of  $\Delta$  production in neutral current interactions can be estimated from the data, using the sample of reconstructed  $\pi^0$  decays. Most  $\nu_\mu$  events can be easily identified by their penetration into the veto region when exiting muons fire the veto, or by muons stopping in the inner detector and producing a Michel electron after a few microseconds.

## 5. SIGNAL SEPARATION FROM THE BACKGROUND

Particle identification (PID) is performed by different algorithms that use the difference in characteristics of the Cerenkov and scintillation light associated with electrons, muons, protons or  $\pi^0$ 's, as shown in Figure 3. These algorithms in-

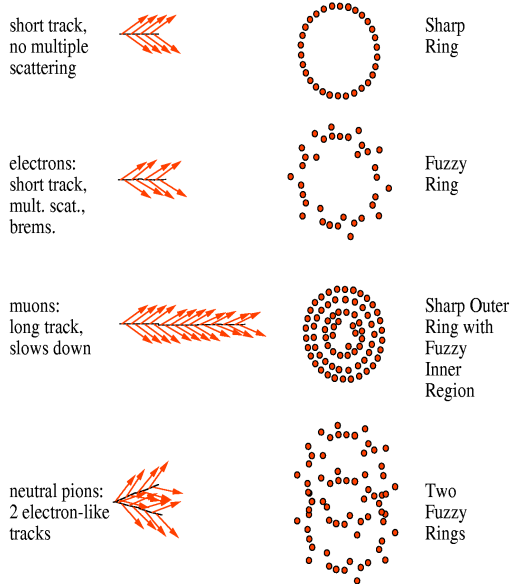


Figure 3. Cartoon showing how particle identification acquires an input from the Cerenkov rings. From the top to the bottom, the rings are: an ideal particle, an electron, a stopping muon, and  $\pi^0$ .

clude a maximum likelihood method and boosted decision trees [8]. Figure 4 shows the logarithm of the likelihood ratio formed from fitting neutral current  $\pi^0$  candidates under a single electron ring hypothesis and a two ring hypothesis where the kinematics are fixed to give the nominal  $\pi^0$  mass. Electron-like events should have larger positive values, while  $\pi^0$ 's should have negative values. The events are selected by requiring no decay

electrons following the primary interaction, and requiring the veto to have less than six hits to ensure there is no cosmic muon contamination and the tank to have greater than 200 hits to suppress decay electrons from cosmic muons. The events are then fit under the single electron and muon ring hypotheses and a ratio is formed with the resulting likelihoods. Events with likelihood ratios favoring the muon hypothesis are rejected. The event is then fit with two ring fits, both with the mass free and fixed to the nominal  $\pi^0$  mass. In the case from Figure 3, separation between  $\pi^0$

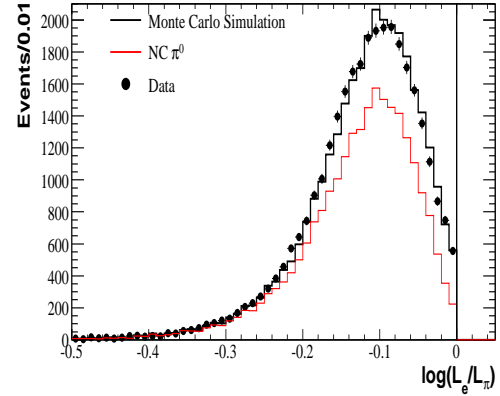


Figure 4. (Preliminary) The logarithm of the likelihood ratio formed from fitting neutral current  $\pi^0$  candidates under a single electron ring hypothesis and a two ring hypothesis. The data are the black points, the black line is Monte Carlo simulated neutrino interactions, while the red line is the subset of these events which have at least one  $\pi^0$  in the final state.

and  $\nu_e$  candidates is achieved. Similar PID separation is performed between electrons and other types of detected events. An example of a boosted decision tree where the muon/electron separation was measured with cosmic ray muons and associated electrons is given in [9]. The PID removes  $\sim 99.9\%$  of  $\nu_\mu$  CCQE interactions,  $\sim 99\%$  ef-

fective  $\pi^0$  producing interactions, and preserves a high efficiency for  $\nu_e$  interactions. An optimized PID is expected to allow a small contamination of an oscillation signal with mis-identified  $\pi^0$  ( $\sim 83\%$ ),  $\Delta$ -decays ( $\sim 7\%$ ), and  $\nu_\mu$  CCQE events ( $\sim 10\%$ ).

## 6. BLIND ANALYSIS STRATEGY AND CROSS-CHECKS

MiniBooNE is conducting a blind analysis in order to complete an unbiased oscillation search. That means that the region where the oscillation  $\nu_e$  candidates are expected is closed for the analysis. In the example given in Figure 4, the mass from the fit is required to be greater than  $50 \text{ MeV}/c^2$ . The likelihood ratio of the single electron fit and the fixed mass two ring fit is required to favor the  $\pi^0$  hypothesis. The latter two requirements are for blindness, in order to keep the region with potential oscillation  $\nu_e$  candidates out of the analysis reach until the final set of selection cuts is formed and the PID is optimized. In practice, the MiniBooNE analysis cannot use its own data to verify PID algorithms with an oscillation-like  $\nu_e$  data sample. However, an important cross-check of electron event reconstruction and particle identification comes from NuMI events observed in the MiniBooNE detector. Neutrinos produced by the decay of mesons moving along the NuMI beamline and in the vicinity of the NuMI target may reach the MiniBooNE detector. NuMI events consist of  $\nu_e$ ,  $\nu_\mu$ ,  $\pi^\pm$ ,  $\pi^0$  and  $\Delta$  over the range of energies relevant to the appearance analysis. A kaon and non-kaon fractions in NuMI Monte Carlo are extracted from a fit to the data. Such Monte Carlo is then compared to our Monte Carlo prediction. The NuMI sample therefore allows an independent check of the MiniBooNE PID algorithms performance in isolating  $\nu_e$ . Other important checks are performed with either MiniBooNE or external data. A complete list of cross-checks is given in Table 1.

Table 1

The MiniBooNE analysis is verified by different experimental cross-checks for each event class relevant to  $\nu_e$  appearance search.

$K^+$	HARP [10], External Data MiniBooNE Data
$K^0$	E910 [11], External Data MiniBooNE Data
$\mu$	MiniBooNE Data
$\pi^0$	NuMI, MiniBooNE Data
Other ( $\Delta$ , etc)	NuMI, MiniBooNE Data

## 7. REMAINING STEPS IN THE OSCILLATION SEARCH

When the final set of the analysis cuts is determined and associated systematics evaluated, the data sample that potentially contains the oscillation candidates will be un-blinded. The composition of the final sample will be predicted by the MiniBooNE Monte Carlo simulation, with Monte Carlo sample filtered through the same set of PID cuts. If MiniBooNE confirms the LSND result, an excess of events in the data distributions when compared to Monte Carlo will be observed. The final event sample will be evaluated using a  $\chi^2$  function

$$\chi^2 = \sum_{i=1} (O_i - P_i)(C_{ij})^{-1}(O_j - P_j), \quad (1)$$

applied to the data and Monte Carlo energy distribution of the oscillation candidates.  $O_i$  is the number of observed events in an energy bin  $i$ .  $P_i$  is the Monte Carlo prediction that takes into account oscillation parameters ( $\sin^2 2\theta, \Delta m^2$ ). The covariance matrix  $C_{ij}$  account for the statistical and systematic uncertainties in the energy bins. Systematic errors are associated with neutrino flux, neutrino cross sections, and the detector model.

The flux prediction has the uncertainties corresponding to the production of  $\pi$ ,  $K$ , and  $K_L$  particles in the MiniBooNE target. These uncertainties are quantified by a fit to external data sets from previous experiments on meson production. The cross section uncertainties are eval-

uated by continuously varying underlying cross section model parameters in the Monte Carlo constrained by MiniBooNE data. Uncertainties on the parameters modeling the optical properties of the oil in the MiniBooNE detector are constrained by a fit to the calibration sample of Michel electrons. The uncertainties are currently being evaluated.

## 8. CONCLUSION

The MiniBooNE experiment will confirm or refute the LSND oscillation signal with approximately  $6 \times 10^{20}$  protons on target collected for the analysis. The oscillation appearance analysis is underway, with current work on the systematic error evaluation that combines the errors from the  $\nu$  flux,  $\nu$  cross-sections, and the detector modeling.

The MiniBooNE Collaboration: A.A. Aguilar-Arevalo, A.O. Bazarko, S. J. Brice, B.C. Brown, L. Bugel, J. Cao, L. Coney, J.M. Conrad, D.C. Cox, A. Curioni, Z. Djurcic, D.A. Finley, B.T. Fleming, R. Ford, F. Garcia, G.T. Garvey, A. Green, C. Green, T.L. Hart, E. Hawker, R. Im-lay, R.A. Johnson, P. Kasper, T. Katori, T. Kobilarcik, I. Kourbanis, S. Koutsoliotas, J.M. Link, Y. Liu, Y. Liu, W.C. Louis, K.B.M. Mahn, W. Marsh, P. Martin, G. McGregor, W. Metcalf, P.D. Meyers, F. Mills, G.B. Mills J. Monroe, C.D. Moore, R.H. Nelson, P. Nienaber, S. Ouedraogo, R.B. Patterson, D. Perevalov, C.C. Polly, E. Prebys, J.L. Raaf, H. Ray, B.P. Roe, A.D. Russell, V. Sandberg, R. Schirato, D. Schmitz, M.H. Shaevitz, F.C. Shoemaker, D. Smith, M. Sorel, P. Spentzouris, I. Stancu, R.J. Stefanski, M. Sung, H.A. Tanaka, R. Tayloe, M. Tzanov, M.O. Wascko, R. Van de Water D.H. White, M.J. Wilking, H.J. Yang, G.P. Zeller, E.D. Zimmerman.

## REFERENCES

1. B.T. Cleveland *et al.*, *Astrophysics. J.* 496 (1998) 505.; J.N. Abdurashitov *et al.*, *Phys. Rev. C.*, 60 (1999) 055801.; W. Hampel *et al.*, *Phys. Lett. B* 447 (1999) 127.; Q.R. Ahmed *et al.*, *Phys. Rev. Lett.* 87, (2001) 071301.; Q.R. Ahmed *et al.*, *Phys. Rev. Lett.* 89, (2002) 011301.; S.N. Ahmed *et al.*, *Phys. Rev. Lett.* 92, (2004) 181301.
2. K. Eguchi *et al.*, *Phys. Rev. Lett.* 90, (2003) 021802.; K. Eguchi *et al.*, *Phys. Rev. Lett.* 94, (2005) 081801.
3. S.H. Hirata *et al.*, *Phys. Lett. B* 280 (1992) 146.; Y. Fukuda *et al.*, *Phys. Lett. B* 335 (1994) 237.; S. Fukuda *et al.*, *Phys. Rev. Lett.* 81 (1998) 1562.
4. M.H. Ahn *et al.*, *Phys. Rev. Lett.* 90 (2003) 041801.
5. C. Athanassopoulos *et al.*, *Phys. Rev. Lett.* 75 (1995) 2650.; C. Athanassopoulos *et al.*, *Phys. Rev. D* 64 (2001) 112007.
6. M. Sorel, J.M. Conrad, and M. Shaevitz, *Phys. Rev. D* 70 (2004) 073004.
7. D. Casper, *Nucl. Phys. Proc. Suppl.* 112 (2002) 161.
8. B.P. Roe *et al.*, *Nucl. Inst. Meth. A* **543**, 577 (2005).; H-J. Yang, B.P. Roe and J. Zhu, *Nucl. Inst. Meth. A* **555**, 370 (2005).
9. Z. Djurcic, *AIP Conf. Proc.* 842 (2006) 828, arXiv:hep-ex/0601014.
10. The HARP Experiment at CERN, <http://harp.web.cern.ch/harp/>.
11. The E910 Experiment at BNL, <http://www.phy.bnl.gov/~e910/html/home.html>.